RSC Advances

ROYAL SOCIETY OF CHEMISTRY

www.rsc.org/advances

A ratiometric nanosensor based on fluorescent carbon dots for label-free and highly selective recognition of DNA

Shan Huang[a], Lumin Wang[a], Fawei Zhu[a], Wei Su[a], Jiarong Sheng[a], Chusheng Huang[a], and Qi Xiao[a,b,*]

[a] *College of Chemistry and Materials Science, Guangxi Teachers Education University, Nanning 530001, P. R. China*

[b] *State Key Laboratory of Virology, Wuhan University, Wuhan 430072, P. R. China*

* Corresponding author. Tel.: +86 771 3908065; Fax: +86 771 3908065;

E-mail address: qi.xiao@whu.edu.cn

Abstract: A ratiometric nanosensor for label-free and highly selective recognition of DNA was reported in this work, by employing fluorescent carbon dots (CDs) as the reference fluorophore and ethidium bromide (EB), a specific organic fluorescent dye toward DNA, playing the role as both specific recognition element and response signal. Fluorescent CDs were synthesized through microwave irradiation technique. When EB was present, the fluorescence of CDs was quench effectively due to the electron transfer process between CDs and EB, while the fluorescence of EB was increased partially without fluorescence resonance energy transfer under same excitation wavelength. Upon the addition of DNA, the fluorescence of EB was enhanced dramatically but the fluorescence intensity of CDs stayed almost constant, leading to a ratiometric detection of DNA. This fluorescent nanosensor exhibited good sensitivity, a broad dynamic linear range of 1.0 μM ~ 100 μM, and low detection limit down to 0.47 μM. The relative standard deviation for 30 μM DNA was 0.2% (n = 5). The present ratiometric nanosensor also showed high accuracy and excellent selectivity for DNA over some chemical substances, amino acids, nucleotides, proteins, and RNA. The proposed method was applied to the determination of DNA in synthetic samples with satisfactory results. The proposed DNA detection method was quite simple, rapid and convenient due to the elimination of the modification and separation procedures. The possible fluorescence quenching mechanism was further investigated.

Keywords: Ratiometric nanosensor, Fluorescent carbon dots, Ethidium bromide, DNA, Recognition

1. Introduction

Fluorescent carbon dots (CDs), a new type of zero-dimensional nanomaterials in carbon family, have attracted increasing attention in recent years.[1–4] Compared with some classic semiconductor quantum dots (QDs) with heavy metal cores and fluorescent molecules, CDs further possess numerous chemical/physical merits such as less-expensive cost, simple synthesis route, low cytotoxicity, good biocompatibility, high photo and chemical stability, and tunable excitation and emission spectra.[5–7] These properties make CDs to be excellent fluorescent probes for some chemical and biological assay.[8–10] Recently, some metal ions and important molecules were detected based on the unidirectional fluorescence variation of CDs.[11–18] Vedamalai et al. have developed a novel luminescence sensing system for Cu^{2+} detection, based on the fluorescence enhancement of CDs which prepared from o-phenylenediamine.[11] Chen's group have proposed a solid-phase synthesized N-doped CDs for sensitive and selective probing Fe^{3+} in living cells.[12] Costas-Mora and coworkers have reported an sensitive and selective detection of methylmercury with the fluorescence quenching of fluorescent CDs.[13] Ahmed et al. further used the fluorescent CDs for sensitive and selective detection of tannic acid in wines.[17] Yang's group have explored specific and selective detection approach for tetracyclines by fluorescence quenching of CDs.[18] However, this unidirectional fluorescence variation of CDs could be easily affected by foreign substances and subsequently deterred the practical application of CDs greatly. In order to expand the analytical applications of CDs fluorescent nanosensor, new strategies should be explored urgently to improve the sensitivity and selectivity of CDs.

Fortunately, a novel detection strategy based on the reversible fluorescence "ON-OFF-ON" change of QDs has been explored and ignited widespread interest.[19–21] Recently, this mode based on CDs was also established to detect some ions (such as Hg^{2+}, Cu^{2+}, Pb^{2+}, Cr^{6+}, $C_2O_4^{2-}$, PO_4^{3-}, and $P_2O_4^{7-}$, etc.),[22–27] and biochemical substances (for instance, ascorbic acid, hydrogen sulfide, biothiols, L-cysteine, melamine, and DNA etc.).[25,28–32] A major limitation is that such single-wavelength-based detecting signal is easily interfered with various factors, such as the concentration change of sensors, optical path length, drift of light source or detector, and environmental conditions of the complex samples, which otherwise prevent the precise and quantitative determination. Ratiometric fluorescent sensors, which use the intensity ratio of two or

more well-resolved wavelengths, can efficiently overcome the above limits by self-calibration of two or more emission intensities and thus have attracted significant attention in recent years.[33–35] Recently, CDs-based dual-emission nanohybrid materials are prepared and used as a ratiometric fluorescent probe for different substances.[36–41] Wu's group have developed CDs-based ratiometric fluorescent sensor for intracellular pH and hydrogen sulfide sensing and mapping.[36,37] Liu et al. developed a novel nanohybrid ratiometric fluorescence probe comprised of CDs and CdSe/ZnS QDs for visual Hg^{2+} sensing.[39] Tian and coworkers also prepared CDs-based ratiometric fluorescent probe for *in vivo* imaging of cellular Cu^{2+} and superoxide anion.[40,41] As a matter of fact, this ratiometric fluorescence measurements can not only drastically improve the sensitivity of the detection but also efficiently avoid interferences from background fluorescence, because the ratio of the fluorescence intensities at two different wavelengths is independent of the probe concentration and the inhomogeneous distribution, the fluctuation of light-source intensity, and the sensitivity of instruments.

Inspired by these facts, we fabricated a selective and sensitive fluorescence nanosensor for ratiometric determination of DNA by simple mixing blue-emission fluorescent CDs and red-emission ethidium bromide (EB). As shown in Scheme 1, the fluorescence of CDs could be efficiently quenched by EB due to the electron transfer process between CDs and EB, while the fluorescence of EB was enhanced partially without fluorescence resonance energy transfer under same excitation wavelength, resulting in the distinct fluorescence color change from blue to dark red. Upon the addition of DNA, the fluorescence of EB was increased significantly because of the strong intercalating interaction between EB and DNA, while CDs were almost insensitive to DNA, which led to the fluorescence intensity variation as well as the distinct fluorescence color change from dark red to bright red which could be obviously observed by the naked eye. In this design, fluorescent CDs were synthesized through microwave irradiation technique and covalent immobilization of the probe molecules was not required. The selectivity and sensitivity of this ratiometric fluorescent nanosensor to DNA were carefully investigated. The feasibility of such ratiometric fluorescent nanosensor for DNA determination in synthetic samples was also investigated. Such hybridized ratiometric nanosensor has been demonstrated label-free, highly sensitive and selective for practical application such as on-site and visual detection of DNA.

2. Materials and methods

2.1 Materials

Polyethylene glycol 1500 (PEG 1500), glycerine, and L-serine were purchased from Sigma (St. Louis, MO, USA). EB, calf thymus DNA, amino acids, nucleotides, and RNA were obtained from Sinopharm Chemical Reagent Factory (Shanghai, China). All other reagents were of analytical-reagent grade and used as received. Ultrapure water with a resistivity of 18.2 MΩ cm was produced by passing through a RiOs 8 unit followed by a Millipore-Q Academic purification set (Millipore, Bedford, MA, USA) and used throughout the whole experiments.

2.2 Apparatus

The fluorescent CDs were prepared by using CEM Discover Benchmate microwave reactor (CEM, USA). UV-vis absorption spectra were measured on Cary 100 UV-vis spectrophotometer (Agilent Technologies, Inc., Australia). Fluorescence spectra and intensities were performed on Perkin-Elmer LS-55 luminescence spectrometer (PerkinElmer, USA) equipped with a 20KW xenon discharge lamp as light source. Quartz cells (1.0 cm path-length) were used for all measurements. FT-IR spectra were recorded on Nicolet iS10 spectrometer (Thermo, USA) equipped with ZnSe attenuated total reflection (ATR) accessory, a deuterated triglycine sulfate detector, and a KBr beam splitter. The time-resolved fluorescence decay traces were recorded with a Fluorolog-3 system (Horiba Jobin Yvon, France) by using an excitation wavelength of 374 nm. High-resolution transmission electron microscopy (TEM) images of CDs were taken by a JEM 2011FEF high-resolution transmission electron microscope (JEOL Ltd., Tokyo, Japan). All pH measurements were made with a basic pH meter PB-10 (Sartorius Scientific Instruments Co., Ltd., Beijing, China).

2.3 Preparation of CDs using the microwave irradiation technique

The fluorescent CDs were synthesized according to the method reported previously with minor modification.[42] In a typical synthesis, 1.0 g PEG 1500 and 15 mL glycerine were mixed and pretreated with microwave reactor under 200 W and 160 °C for 15 min in order to form clean and homogeneous solution. When the mixture solution naturally cooled down to 50 °C, 1.0 g L-serine powder was injected into the mixed solution following. Then, the mixture was further treated by

microwave reactor at 200 W and 180 °C for 10 min. The obtained mixture was cooled to room temperature. The color of the solution changed to brown and the solution exhibited strong blue fluorescence under 365 nm UV irradiation. The fluorescent CDs were purified by dialyzing against ultrapure water using dialysis membranes with 1000 MWCO for 3 days. The fluorescent CDs solution was then concentrated by rotary evaporator to 5 mL and stored at 4 °C for use.

2.4 Quantum yield measurement

The relative quantum yield (QY) of fluorescent CDs was measured according to the established procedure.[43,44] Quinine sulfate was chosen as the fluorescence standard and the reported QY of quinine sulfate in 0.1 M H_2SO_4 was 54% with 360 nm excitation. Absolute values are calculated using the standard reference sample that has a fixed and known QY value. To minimize the re-absorption effects, absorbencies in the 1.0 cm fluorescence cuvette were kept in the range of 0.01 to 0.1 at the excitation wavelength of 360 nm. The QY of CDs was determined at the excitation wavelength of 375 nm by using the following equation:[35]

$$Q_X = Q_S \frac{I_X}{I_S} \frac{A_S}{A_X} \left(\frac{\eta_X}{\eta_S} \right)^2 \quad (1)$$

Where Q is the QY, I is the measured integrated fluorescence intensity, A is the absorbance at the excitation wavelength, and η is the refractive index of the solvent, respectively. The subscripts "s" and "x" refer to the fluorescence standard with known QY and the sample with unknown QY, respectively.

2.5 Preparation of synthetic samples

For synthetic samples detection, seven samples were prepared by mixing the standard solutions of different solution with different concentrations in the reaction system. The concentrations of $CaCl_2$, $MgCl_2$, $FeSO_4$, and $ZnCl_2$ in sample 1 were 500 μM, 500 μM, 100 μM, and 100 μM, respectively. The concentrations of ascorbic acid (AA), oxidized glutathione (GSSG), reduced glutathione (GSH), L-Tyrosine, and L-Aspartic acid in sample 2 were 300 μM, 300 μM, 300 μM, 500 μM, and 500 μM, respectively. The concentrations of L-Asparagine, L-Arginine, L-Threonine, L-Phenylalanine, and L-Proline in sample 3 were all 500 μM. Sample 4 contained 500 μM L-Glycine, 500 μM L-Glutamine, 500 μM L-Cysteine, 500 μM L-Serine, and 80 μM

L-Methionine. Sample 5 contained 500 μM L-Valine, 500 μM L-Histidine, 500 μM L-Lysine, 500 μM L-Alanine, and 70 μM L-Glutamic acid. The concentrations of guanine, adenine, cytosine, and thymine in sample 6 were all 500 μM. Sample 7 contained 50 μM trypsin, 50 μM lysozyme, 10 μM bovine serum albumin (BSA), and 10 μM human serum albumin (HSA). Different amounts of DNA standard solution were added into the reaction system. The final concentrations of DNA were 5 μM and 10 μM, respectively. The recovery of DNA in synthetic samples was examined by the proposed strategy.

2.6 Procedures for DNA determination

As depicted in Scheme 1, first, 20 μL CDs solution, 1.5 mL phosphate buffer (pH 4.0) and appropriate aliquot of EB solution were transferred into a 5 mL eppendorf tube. The mixture was thoroughly stirred and finally diluted to 5 mL with ultrapure water. After 3 min of the reaction at room temperature, the fluorescence spectra were measured for the selection of EB concentration.

For DNA detection, 1.5 mL phosphate buffer (pH 8.0), 30 μL of 30 mM of EB solution and appropriate aliquot of DNA solution were transferred into a 5 mL eppendorf tube and the mixture was thoroughly stirred. Then, 20 μL CDs solution was added into the mixture and finally diluted to 3 mL with ultrapure water. After 10 min incubation at room temperature, the fluorescence spectra of the mixture solution were measured for the quantitative analysis of DNA. When the samples were determined, the DNA standard solution was substituted by the prepared sample solution described in Section 2.5.

The fluorescence spectra were recorded at excitation wavelength of 375 nm, and the band-slits of excitation and emission were set as 10.0 nm and 5.0 nm, respectively. The fluorescence spectra were recorded from 390 nm to 680 nm, the fluorescence intensities of CDs at 424 nm and EB at 592 nm was used for quantitative analysis of DNA.

3. Results and discussion

3.1 Spectral characterization of CDs

The fluorescent CDs were prepared by facile and economic microwave irradiation by using L-serine as the carbon source, PEG 1500 and glycerine as the co-reactant. The microwave irradiation firstly caused the dehydration and the pyrolysis of these precursors, and then forced

them to break into small fluorescent CDs. So, the microwave irradiation time and the reaction temperature could easily influence both the size and the emission color of CDs.

As shown in Fig. 1A, CDs exhibited broad absorption bands from 200 nm and 450 nm in the typical UV-vis absorption spectrum. Like most fluorescent carbon nanomaterials, an obvious absorption peak around 340 nm, which was ascribed to the $n - \pi^*$ electronic transition of CDs, was likely originated from the trapping of excited state energy by the surface states that led to strong fluorescence.[30] Moreover, the fluorescence spectra indicated that CDs exhibited an obvious, narrow, almost symmetrical fluorescence spectrum with a strong emission peak at 447 nm with an excitation wavelength of 375 nm, with a Stokes shift of 72 nm. From the digital pictures inserted in Fig. 1A, the diluted CDs solution was pale yellow under ambient daylight but exhibited very intense blue emission under UV light (365 nm), which further demonstrated the strong blue fluorescent property of CDs observed by naked eye.

Moreover, as observed from other carbon-based QDs, the as-prepared CDs also exhibited an excitation-dependent fluorescent behavior.[25] As indicated in Fig. 1B, with the excitation wavelength changed from 340 nm to 390 nm, the maximum fluorescence intensity of CDs was first increased and then decreased, but the maximum emission peak position of CDs showed an obvious redshift continuously. These results elucidated that the maximum excitation wavelength and the maximum emission wavelength of CDs were at 375 nm and 447 nm, respectively. Such excitation-dependent fluorescent behavior was related to the different surface states of carbon-based QDs.[14] The corresponding surface state emissive trap was dominant under different excitation wavelength, which resulted in the excitation-dependent fluorescent behavior.

FT-IR spectrum was acquired to identify the surface functional groups present on CDs. As shown in Fig. 2A, the absorption peaks at 3382 cm^{-1} and 2939 cm^{-1} were assigned to the stretching vibrations of O–H and C–H bonds, respectively. The absorption peaks at 560, 675, 1406, and 1459 cm^{-1} were attributed to the bending vibrations of C–H bonds, and the absorption peaks at 1042 and 1110 cm^{-1} correspond to the C–O stretching vibrations. The stretching vibration of C=O bonds around 1637 cm^{-1} was also detected, revealing that the obtained CDs were equipped with –COOH and –OH groups.[23,26] These results demonstrated that the as-prepared CDs exhibited excellent water solubility and could be easily functionalized with biomolecules due to the oxygen-containing functional groups, which was conducive to the applications of CDs in the area

of the fluorescence probes.

These CDs were nearly spherical with good size distribution and excellent monodispersity, and the average sizes of CDs were around 4 ~ 8 nm (Fig. 2B). The relative QY of CDs was examined to be about 12.1% at 375 nm excitation in reference to quinine sulfate whose QY was 54% in 0.1 H_2SO_4 solution (Fig. S1). The stability of CDs was also investigated by long-time monitoring of fluorescence intensity at room temperature, and it should be pointed out that these CDs exhibited high photostability at room temperature. In addition, these CDs exhibited negligible variation of fluorescence intensity and no obvious photobleaching loss at 447 nm under visible light for 25 days (Fig. S2). Even after being stored for three months in air, there was no observation of any floating or precipitated nanoparticles in solution, showing their advantages for potential applications. Furthermore, the influence of pH on the fluorescence property of CDs was also investigated (Fig. S3). The fluorescence intensity of CDs decreased upon regulating pH value from 3 to 12, and the maximum emission wavelength gradually blue-shifted with increasing pH value, which indicated that the fluorescence property of CDs strongly depended on the pH value.

3.2 Fluorescence quenching effect of EB on CDs

In order to understand the response rate between CDs and EB, the time-dependent fluorescence changes of CDs–EB system were evaluated. As indicated in Fig. S4, when 300 μM EB solution was added into the CDs solution, the fluorescence of CDs was quenched within 1 min of the contact time, which meant that the response rate was rapid. The fluorescence quenching reached a steady state during 2 min. A further increase in time did not lead to any further detectable quenching of the fluorescence of CDs. Thus, the fluorescence intensity of CDs–EB system was recorded after the addition of EB for 3 min.

Furthermore, the influence of different pH values on the fluorescence intensity reflecting the interaction between CDs and EB was investigated from pH 3.0 to 12.0. The variation in fluorescence intensity between CDs and CDs–EB system was shown in Fig. 3A. It was found that the change in fluorescence intensity gradually increased with the increase of pH value from 3.0 to 4.0. When pH value was higher than 4.0, the change in fluorescence intensity decreased continuously. The maximum change in fluorescence intensities was observed when pH value was 4.0. Therefore, phosphate buffer with pH 4.0 was chosen for fluorescence quenching experiments.

Upon addition of EB into CDs solution, EB could adsorb onto the surface of CDs and then quench the fluorescence of CDs. In order to validate the exact quenching mechanism between CDs and EB, the control experiments between CDs alone, EB alone, and CDs–EB system were taken. As indicated in Fig. 3B, the fluorescence intensity of EB in CDs–EB system were almost the same with the fluorescence intensity of EB alone under the same excitation wavelength of 375 nm, indicating no fluorescence resonance energy transfer occurred between CDs and EB. As a result, the fluorescence of CDs was quenched by EB through electron transfer process in several minutes.

Fig. 4 showed the fluorescence spectra of CDs with different concentration of EB. It could be seen that, when EB was added into CDs solution, the fluorescence intensity of CDs was quenched dramatically, while the fluorescence intensity of EB was increased gradually. In addition, with the increase of the concentration of EB from 0 to 300 μM, the emission peak position of CDs was blue-shifted from 447 nm to 424 nm, which suggested that the surface bond might be formed between CDs and EB. Such interaction would undermine the stability and the polarity of the fluorescent properties of surface functional groups, leading to the fluorescence quenching of CDs.[45] The quenching of the fluorescence intensity of CDs by EB can be described according to the Stern-Volmer equation:

$$\frac{I_0}{I} = 1 + K_{SV}[Q] \qquad (2)$$

where I_0 and I are the fluorescence intensity of CDs in the absence and presence of EB, respectively. [Q] is the concentration of EB and K_{SV} is the Stern-Volmer quenching constant, respectively. A typical Stern-Volmer plot was inserted in Fig. 4, and a calibration curve of $I_0 / I = 1 + 1.0 \times 10^4$ [EB] was obtained. Good linearity between the I_0 / I and the EB concentrations was obtained over the concentration range from 1.0 μM to 300 μM. From the slope of the linear plot, the quenching constant K_{sv} was calculated to be 1.0×10^4 L mol^{-1}, with a detection limit ($3\sigma / s$, σ and s are the standard deviation of 12 blank measurements and the slope of the calibration curve, respectively) of 0.6 μM and a correlation coefficient of 0.9990. Moreover, the precision expressed as the relative standard deviation, attained from a series of 12 standard samples without EB, was 0.2%.

3.3 Ratiometric fluorescence variation assay of DNA

The influence of DNA on the CDs–EB system was further investigated. Fig. 5A depicted the fluorescence spectra of CDs alone, CDs–DNA, CDs–EB and CDs–EB–DNA under the same experimental conditions. As shown in this figure, when excited at 375 nm, CDs exhibited strong fluorescence at 447 nm (curve a). As expected, once EB was introduced, the fluorescence of CDs was significantly decreased and the fluorescent peak position was blue-shifted (curve c and curve d), together with the increase of the fluorescence intensity of EB, due to the interaction between CDs and EB. Upon addition of DNA, EB molecules interacted with DNA via strong and specific intercalative interaction between EB and DNA, which thus resulted in the increase of the fluorescence intensity of EB (curve e). However, the fluorescence intensity of CDs was almost not changed, which subsequently generated the ratiometric fluorescence effect. In order to get rid of the possible adverse impact on the fluorescence intensity caused by DNA, DNA was also employed into the CDs solution as a contrast. The intense fluorescence indicated that DNA caused negligible effect on the fluorescence intensity of CDs (curve b). The evolution of fluorescence intensity of the four solutions mentioned above demonstrated the feasibility of this strategy. Therefore, we speculated that a ratiometric fluorescence method could be proposed for the determination of DNA.

3.4 Optimization of the experimental conditions for DNA determination

The parameters including addition sequence of reagents, incubation time, media pH value and EB concentration are optimized for CDs–EB–DNA system. To increase the sensitivity of this ratiometric nanosensor, the addition sequence of reagents was investigated. As shown in Fig. S5, different addition sequences could affect the fluorescence intensity of EB obviously, and the optimal addition sequence of this system was phosphate buffer, EB, DNA and CDs solution. At room temperature, the time dependent fluorescence of CDs–EB–DNA system was also investigated. As shown in Fig. S6, the fluorescence of CDs was constant, and the fluorescence of EB was obviously increased by DNA within 5 min and almost lasted for more than 80 min. To ensure the consistency throughout the experiment and obtain stable signal, 10 min was chosen as the optimum incubation time for CDs–EB–DNA system.

In addition, the stability of DNA and the fluorescence intensity of CDs are closely related to the pH value of the solution. Taking this point into consideration, pH values changing from 4.0 to 12.0

were systemically investigated to seek the optimum condition for CDs–EB–DNA system. Fig. 5B showed fluorescence intensity of CDs–EB system in the absence and presence of DNA in different pH media. It seemed that the addition of DNA did not cause significant change to the CDs fluorescence but resulted in the tremendous enhancement of the EB fluorescence. The fluorescence intensity ratio of EB and CDs, which was defined as I_{EB} / I_{CDs}, was also exhibited in Fig. 5C. Under the slightly alkaline environment (especially when pH value was 8.0), the I_{EB} / I_{CDs} value showed much greater enhancement. Therefore, phosphate buffer with pH 8.0 was chosen for further DNA detection.

Besides, the effect of EB concentration on CDs–EB–DNA system was also investigated. It was obvious that the fluorescence intensity ratio of EB and CDs increased gradually with increasing the concentration of EB, because the fluorescence intensity of CDs was decreased while the fluorescence intensity of EB was increased. Meanwhile, the dynamic linear range and the sensitivity of DNA determination could be increased with the addition of higher concentration of EB. According to the above analysis, 300 μM of EB was chosen as the optimum concentration.

3.5 Detection of DNA

Under the optimum conditions, the fluorescence spectra of CDs–EB system in the presence of different amounts of DNA were shown in Fig. 6. As displays in this figure, with increasing the concentration of DNA, the fluorescence intensity of EB increases gradually but the fluorescence intensity of CDs kept almost constant. The plot of the fluorescence intensity ratio of EB and CDs against the concentration of added DNA was shown as an inset in Fig. 6. It was clear that the fluorescence intensity ratio of EB and CDs exhibited a linear response to the DNA concentration in the range of 1.0 μM ~ 100 μM, the calibration curve was express as I_{EB} / I_{CDs} = 0.71 + 0.021 [DNA]. The limit detection (3σ / s) for DNA was 0.47 μM, where σ represented the standard deviation of 12 blank measurements, and s was the slope of the calibration curve. The repeatability of the detection system was investigated by operating five repeated measurements of 30 μM DNA, and the relative standard deviation (R.S.D.) was found to be 0.2%, which suggested the reliability of the proposed ratiometric fluorescent nanosensor.

3.6 Influences of potential interfering substances and synthetic sample determination

To demonstrate the applicability of this approach for DNA determination in biological samples, the influence of some chemical substances, amino acids, nucleotides, proteins, and RNA were investigated. As shown in Table 1, if the coexisting substances caused a relative error of less than ± 5% in the fluorescence intensity ratio of EB and CDs, they were considered to have no interference with DNA determination. It was seen from Table 1 that these coexisted substances showed almost no distinct interferences on the determination of 10 μM DNA. Furthermore, 30 μM BSA, 30 μM HSA, 90 μM trypsin, 100 μM lysozyme, and 40 μM RNA did not affect the detection of 10 μM DNA in the given conditions. These data revealed that the proposed method might be applied to the DNA detection in biological samples.

To confirm the feasibility, the present method was used to detect DNA in synthetic samples which contained some chemical substances, 17 amino acids, 4 nucleotides, and 4 proteins. As indicated in Table 2, the values found for these synthetic samples were identical with the expected values and the recoveries were from 97.2% to 102.1%, which indicated the suitability of DNA determination in the mixture of these substances.

3.7 Possible fluorescence quenching mechanism

The fluorescence quenching mechanism mainly includes dynamic quenching and static quenching, which can be distinguished by careful examination of the absorption spectra of fluorophore, because the absorption spectra of fluorophore will be changed in the static quenching but will be remained unchanged in the dynamic quenching.[20] So, the UV-vis absorption spectra of CDs, EB, CDs–EB system, the difference absorption spectrum between CDs–EB system and EB, and the summed absorption spectrum between CDs and EB were recorded to reveal the probable fluorescence quenching mechanism of CDs–EB system. As shown in Fig. 7A, the UV-vis absorption spectrum of CDs and the difference absorption spectrum between CDs–EB system and EB was superposed perfectly within the experimental error, and the absorption spectra of CDs–EB system and the summed absorption spectrum of CDs and EB was also overlapped well within the experimental error, which implied that no conjugation or particle-size variation occurred in this dynamic fluorescence quenching process. Furthermore, the UV-vis absorption spectra of DNA, EB, EB–DNA system, and the difference absorption spectrum between EB–DNA system and EB were also used to investigate the intercalation interaction between DNA and EB. As illustrated in

Fig. 7B, the absorption spectrum of EB and the difference absorption spectrum between EB–DNA system and DNA were totally different, indicating the intercalation interaction between DNA and EB.

Moreover, the fluorescence quenching mechanism can also be clarified directly by testing the fluorescence lifetime of fluorophore, since the fluorescence lifetime of fluorophore will be shortened in dynamic quenching but will be unchanged in static quenching.[20] Therefore, the time-resolved fluorescence spectra of CDs alone, CDs–EB system and CDs–EB–DNA system were measured to reveal the possible fluorescence quenching mechanism and to investigate the photophysical properties of these systems. The fluorescence decay curves were well fitted with biexponential equation, and the average decay time was given by the sum of the $\sum b_i\tau_i$ products.[20,46] As shown in Fig. 8, CDs exhibited two fluorescence decay components, τ_1 2.28 ns (36.53%) and τ_2 8.97 ns (63.47%). The corresponding average decay time of CDs was about 6.53 ns. When EB was added into the solution, two fluorescence decay components of CDs were shortened to τ_1 1.62 ns (33.28%) and τ_2 7.61 ns (66.72%). The average decay time of CDs was also decreased to around 5.62 ns. These results further indicated the dynamic quenching of CDs by EB and also confirmed the occurrence of electron transfer process between CDs and EB. After the addition of DNA into CDs–EB system, two fluorescence decay components of CDs were increased to τ_1 1.94 ns (43.21%) and τ_2 8.20 ns (56.79%). However, the average decay time of CDs was decreased slightly, 5.49 ns. These results were highly consistent with the results revealed in Fig. 6. These results also indicated the electron transfer process between CDs and EB and the intercalative interaction between DNA and EB (Scheme 1), which resulted in the ratiometric fluorescence approach for DNA determination.

4. Conclusions

In summary, a novel retiometric fluorescent nanosensor composed of CDs and EB was established for the determination of DNA. The primary advantage of this method was its simplicity, sensitivity and specificity. The fluorescence of CDs was quenched by EB through electron transfer process and no fluorescence resonance energy transfer was occurred between CDs and EB. Then, after the addition of DNA, the fluorescence of EB was increased significantly because of the strong intercalative interaction between EB and DNA, while CDs were almost

insensitive to DNA, leading to a ratiometric detection of DNA. Under the optimum conditions, the present method had a linear range of 1.0 μM ~ 100 μM, with a correlation coefficient of 0.9999. The limit of detection of DNA was 0.47 μM. Some chemical substances, amino acids, nucleotides, proteins, and RNA did not affect the determination of DNA. The presented method has been successfully applied to the determination of DNA in synthetic samples successfully. The possible fluorescence quenching mechanism of this ratiometric fluorescent nanosensor was dynamic quenching.

Acknowledgements

This work was financially supported by the National Natural Science Foundation of China (21203035, 21403039), the Guangxi Natural Science Foundation (2013GXNSFCA019005, 2013GXNSFBA019029), the Scientific Research Foundation of Guangxi Provincial Education Department (ZD2014081), the Innovation Project of Guangxi Graduate Education (YCSZ2014186) and Guangxi Colleges and Universities Key Laboratory of Synthetic and Natural Functional Molecular Chemistry, Guangxi Teachers Education University.

References

[1] C. Fowley, A. P. McHale, B. McCaughan, A. Fraix, S. Sortino and J. F. Callan, Carbon quantum dot–NO photoreleaser nanohybrids for two-photon phototherapy of hypoxic tumors, *Chem. Commun.*., 2015, **51**, 81–84.

[2] Y. Xu, X. H. Jia, X. B. Yin, X. W. He and Y. K. Zhang, Carbon quantum dot stabilized gadolinium nanoprobe prepared via a one-pot hydrothermal approach for magnetic resonance and fluorescence dual-modality bioimaging, *Anal. Chem.*, 2014, **86**, 12122–12129.

[3] S. Y. Lim, W. Shen and Z. Q. Gao, Carbon quantum dots and their applications, *Chem. Soc. Rev.*, 2015, **44**, 362–381.

[4] H. Ding, J. S. Wei and H. M. Xiong, Nitrogen and sulfur co-doped carbon dots with strong blue luminescence, *Nanoscale*, 2014, **6**, 13817–13823.

[5] L. Cheng, Y. M. Li, X. Y. Zhai, B. Xu, Z. Q. Cao and W. G. Liu, Polycation-b-polyzwitterion copolymer grafted luminescent carbon dots as a multifunctional platform for serum-resistant gene delivery and bioimaging, *ACS Appl. Mater. Interfaces*, 2014, **6**, 20487–20497.

[6] L. Wang and H. S. Zhou, Green synthesis of luminescent nitrogen-doped carbon dots from milk and its imaging application, *Anal. Chem.*, 2014, **86**, 8902–8905.

[7] G. Leménager, E. De Luca, Y. P. Sun and P. P. Pompa, Super-resolution fluorescence imaging of biocompatible carbon dots, *Nanoscale*, 2014, **6**, 8617–8623.

[8] X. M. Yang, Y. Zhou, S. S. Zhu, Y. W. Luo, Y. J. Feng and Y. Dou, Novel and green synthesis of high-fluorescent carbon dots originated from honey for sensing and imaging, *Biosens. Bioelectron.*, 2014, **60**, 292–298.

[9] H. Ding, P. Zhang, T. Y. Wang, J. L. Kong, H. M. Xiong, Nitrogen-doped carbon dots derived from polyvinyl pyrrolidone and their multicolor cell imaging, *Nanotechnology*, 2014, **25**, 205604.

[10] X. J. Zhao, W. L. Zhang and Z. Q. Zhou, Sodium hydroxide-mediated hydrogel of citrus pectin for preparation of fluorescent carbon dots for bioimaging, *Colloids Surf. B*, 2014, **123**, 493–497.

[11] M. Vedamalai, A. P. Periasamy, C. W. Wang, Y. T. Tseng, L. C. Ho, C. C. Shih and H. T. Chang, Carbon nanodots prepared from o-phenylenediamine for sensing of Cu^{2+} ions in cells, *Nanoscale*, 2014, **6**, 13119–13125.

[12] H. J. Zhang, Y. L. Chen, M. J. Liang, L. F. Xu, S. D. Qi, H. L. Chen and X. G. Chen, Solid-phase synthesis of highly fluorescent nitrogen-doped carbon dots for sensitive and selective probing ferric ions in living cells, *Anal. Chem.*, 2014, **86**, 9846–9852.

[13] Y. L. Jiang, Q. R. Han, C. Jin, J. Zhang and B. X. Wang, A fluorescence turn-off chemosensor based on N-doped carbon quantum dots for detection of Fe^{3+} in aqueous solution, *Mater. Lett.*, 2015, **141**, 366–368.

[14] R. Z. Zhang and W. Chen, Nitrogen-doped carbon quantum dots: Facile synthesis and application as a "turn-off" fluorescent probe for detection of Hg^{2+} ions, *Biosens. Bioelectron.*, 2014, **55**, 83–90.

[15] I. Costas-Mora, V. Romero, I. Lavilla and C. Bendicho, In situ building of a nanoprobe based on fluorescent carbon dots for methylmercury detection, *Anal. Chem.*, 2014, **86**, 4536–4543.

[16] C. López, M. Zougagh, M. Algarra, E. Rodríquez-Castellón, B. B. Campos, J. C. Esteves da Silva, J. Jiménez-Jiménez and A. Ríos, Microwave-assisted synthesis of carbon dots and its potential as analysis of four heterocyclic aromatic amines, *Talanta*, 2015, **132**, 845–850.

[17] G. H. Ahmed, R. B. Laíño, J. A. Calzón and M. E. García, Fluorescent carbon nanodots for sensitive and selective detection of tannic acid in wines, *Talanta*, 2015, **132**, 252–257.

[18] X. M. Yang, Y. W. Luo, S. S. Zhu, Y. J. Feng, Y. Zhuo and Y. Dou, One-pot synthesis of high fluorescent carbon nanoparticles and their applications as probes for detection of tetracyclines, *Biosens. Bioelectron.*, 2014, **56**, 6–11.

[19] D. W. Huang, C. G. Niu, X. Y. Wang, X. X. Lv and G.M. Zeng, "Turn-On" fluorescent sensor for Hg^{2+} based on single-stranded DNA functionalized Mn:CdS/ZnS quantum dots and gold nanoparticles by time-gated mode, *Anal. Chem.*, 2013, **85**, 1164–1170.

[20] S. Huang, F. W. Zhu, H. N. Qiu, Q. Xiao, Q. Zhou, W. Su and B. Q. Hu, A sensitive quantum dots-based "OFF-ON" fluorescent sensor for ruthenium anticancer drugs and ctDNA, *Colloids Surf. B*, 2014, **117**, 240–247.

[21] S. Huang, F. W. Zhu, Q. Xiao, W. Su, J. R. Sheng, C. S. Huang and B. Q. Hu, A CdTe/CdS/ZnS core/shell/shell QDs-based "OFF–ON" fluorescent biosensor for sensitive and specific determination of L-ascorbic acid, *RSC Adv.*, 2014, **4**, 46751–46761.

[22] X. Cui, L. Zhu, J. Wu, Y. Hou, P. Y. Wang, Z. N. Wang and M. Yang, A fluorescent biosensor based on carbon dots-labeled oligodeoxyribonucleotide and graphene oxide for mercury(II) detection, *Biosens. Bioelectron.*, 2015, **63**, 506–512.

[23] F. Y. Yan, Y. Zou, M. Wang, X. L. Mu, N. Yang and L. Chen, Highly photoluminescent carbon dots-based fluorescent chemosensors for sensitive and selective detection of mercury ions and application of imaging in living cells, *Sens. Actuators B*, 2014, **192**, 488–495.

[24] S. R. Zhang, Q. Wang, G. H. Tian and H. G. Ge, A fluorescent turn-off/on method for detection of Cu^{2+} and oxalate using carbon dots as fluorescent probes in aqueous solution, *Mater. Lett.*, 2014, **115**, 233–236.

[25] M. Zheng, Z. G. Xie, D. Xu, D. Li, P. Du, X. B. Jiang and Z. C. Sun, On−Off−On fluorescent carbon dot nanosensor for recognition of chromium(VI) and ascorbic acid based on the inner filter effect, *ACS Appl. Mater. Interfaces*, 2013, **5**, 13242–13247.

[26] Q. Wang, S. R. Zhang, H. G. Ge, G. H. Tian, N. N. Cao and Y. Q. Li, A fluorescent turn-off/on method based on carbon dots as fluorescent probes for the sensitive determination of Pb^{2+} and pyrophosphate in an aqueous solution, *Sens. Actuators B*, 2015, **207**, 25–33.

[27] H. X. Zhao, L. Q. Liu, Z. D. Liu, Y. Wang, X. J. Zhao and C. Z. Huang, Highly selective

detection of phosphate in very complicated matrixes with an off–on fluorescent probe of europium-adjusted carbon dots, *Chem. Commun.*, 2011, **47**, 2604–2606.

[28] A. W. Zhu, Z. Q. Luo, C. Q. Ding, B. Li, S. Zhou, R. Wang and Y. Tian, A two-photon "turn-on" fluorescent probe based on carbon nanodots for imaging and selective biosensing of hydrogen sulfide in live cells and tissues, *Analyst*, 2014, **139**, 1945–1952.

[29] L. Zhou, Y. H. Lin, Z. Z. Huang, J. S. Ren and X. G. Qu, Carbon nanodots as fluorescence probes for rapid, sensitive, and label-free detection of Hg^{2+} and biothiols in complex matrices, *Chem. Commun.*, 2012, **48**, 1147–1149.

[30] J. Zong, X. L. Yang, A. Trinchi, S. Hardin, I. Cole, Y. H. Zhu, C. Z. Li, T. Muster and G. Wei, Carbon dots as fluorescent probes for "off–on" detection of Cu^{2+} and L-cysteine in aqueous solution, *Biosens. Bioelectron.*, 2014, **51**, 330–335.

[31] H. C. Dai, Y. Shi, Y. L. Wang, Y. J. Sun, J. T. Hu, P. J. Ni and Z. Li, A carbon dot based biosensor for melamine detection by fluorescence resonance energy transfer, *Sens. Actuators B*, 2014, **202**, 201–208.

[32] C. I. Wang, W. C. Wu, A. P. Periasamy and H. T. Chang, Sensitive and selective DNA probe based on "turn-on" photoluminescence of C-dots@RGO, *Anal. Bioanal. Chem.*, 2014, **406**, 6917–6923.

[33] J. L. Yao, K. Zhang, H. J. Zhu, F. Ma, M. T. Sun, H. Yu, J. Sun and S. H. Wang, Efficient ratiometric fluorescence probe based on dual-emission quantum dotshybrid for on-site determination of copper ions, *Anal. Chem.*, 2013, **85**, 6461–6468.

[34] T. Thestrup, J. Litzlbauer, I. Bartholomaus, M. Mues, L. Russo, H. Dana, Y. Kovalchuk, Y. J. Liang, G. Kalamakis, Y. Laukat, S. Becker, G. Witte, A. Geiger, T. Allen, L. C. Rome, T. W. Chen, D. S. Kim, O. Garaschuk, C. Griesinger and O. Gries-beck, Optimized ratiometric calcium sensors for functional in vivo imaging of neurons and T lymphocytes, *Nat. Methods*, 2014, **11**, 175–182.

[35] E. G. Ju, Z. Liu, Y. D. Du, Y. Tao, J. S. Ren and X. G. Qu, Heterogeneous assembled nanocomplexes for ratiometric detection of highly reactive oxygen species *in vitro* and *in vivo*, *ACS Nano*, 2014, **8**, 6014–6023.

[36] F. K. Du, Y. H. Ming, F. Zeng, C. M. Yu and S. Z. Wu, A low cytotoxic and ratiometric fluorescent nanosensor based on carbon-dots for intracellular pH sensing and mapping,

Nanotechnology, 2013, **24**, 365101.

[37] C. M. Yu, X. Z. Li, F. Zeng, F. Y. Zhang and S. Z. Wu, Carbon-dot-based ratiometric fluorescent sensor for detecting hydrogen sulfide in aqueous media and inside live cells, *Chem. Commun.*, 2013, **49**, 403–405.

[38] S. N. Qu, H. Chen, X. M. Zheng, J. S. Cao and X. Y. Liu, Ratiometric fluorescent nanosensor based on water soluble carbon nanodots with multiple sensing capacities, *Nanoscale*, 2013, **5**, 5514–5518.

[39] B. M. Cao, C. Yuan, B. H. Liu, C. L. Jiang, G. J. Guan and M. Y. Han, Ratiometric fluorescence detection of mercuric ion based on the nanohybrid of fluorescence carbon dots and quantum dots, *Anal. Chim. Acta*, 2013, **786**, 146–152.

[40] A. W. Zhu, Q. Qu, X. L. Shao, B. Kong and Y. Tian, Carbon-dot-based dual-emission nanohybrid produces a ratiometric fluorescent sensor for *in vivo* imaging of cellular copper ions, *Angew. Chem. Int. Ed.*, 2012, **51**, 7185–7189.

[41] X. Gao, C. Q. Ding, A. W. Zhu and Y. Tian, Carbon-dot-based ratiometric fluorescent probe for imaging and biosensing of superoxide anion in live cells, *Anal. Chem.*, 2014, **86**, 7071–7078.

[42] Z. Lin, W. Xue, H. Chen and J. M. Lin, Classical oxidant induced chemiluminescence of fluorescent carbon dots, *Chem. Commun.*, 2012, **48**, 1051–1053.

[43] B. De and N. Karak, A green and facile approach for the synthesis of water soluble fluorescent carbon dots from banana juice, *RSC Adv.*, 2013, **3**, 8286–8290.

[44] K. G. Qu, J. S. Wang, J. S. Ren and X. G. Qu, Carbon dots prepared by hydrothermal treatment of dopamine as an effective fluorescent sensing platform for the label-free detection of iron (III) ions and dopamine, *Chem. Eur. J.*, 2013, **19**, 7243–7249.

[45] J. R. Lakowicz, Principles of fluorescence spectroscopy, Springer, New York, 3rd edn, 2006.

[46] A. Orte, J. M. Alvarez-Pez and M. J. Ruedas-Rama, Fluorescence lifetime imaging microscopy for the detection of intracellular pH with quantum dot nanosensors, ACS Nano, 2013, 7, 6378–6395.

Table 1. Effect of coexisting foreign substances for DNA determination [a].

Table 2. Detection of DNA in synthetic samples (n = 5).

Figure Captions

Scheme 1. Principle of DNA determination using CDs-based retiometric fluorescent nanosensor.

Fig. 1. (A) UV-vis absorption spectra of CDs (a), the excitation spectrum of CDs at λ_{em} = 447 nm (b), and the emission spectrum of CDs at λ_{ex} = 375 nm (c). Insert: Photograph of CDs under the radiation of white light (Left) and 365 nm UV lamp (Right). (B) Fluorescence spectra of CDs at different excitation wavelength.

Fig. 2. (A) FT-IR spectrum of CDs. (B) TEM image of CDs.

Fig. 3. (A) Influence of pH value on the fluorescence intensity of CDs alone, the fluorescence intensity of CDs–EB system, and the difference between the CDs alone and CDs–EB system. CDs: 20 μL; EB: 80 μM. (B) The control experiment. CDs alone (a); CDs–EB system (b); EB alone (c). CDs: 20 μL; EB: 150 μM.

Fig. 4. Fluorescence spectra of CDs in different concentrations of EB (a ~ n): 0; 1; 5; 10; 20; 30; 40; 60; 80; 100; 140; 180; 240; 300 μM. Insert: linear relationship between I_0 / I and EB concentration in the range of 1.0 μM ~ 300 μM. CDs: 20 μL; pH: 4.0.

Fig. 5. (A) The fluorescence spectra of CDs alone (a), CDs–DNA (b), CDs–EB (c, d) and CDs–EB–DNA (e). CDs: 20 μL; EB: 100 μM (c) and 300 μM (d, e); DNA: 10 μM (b, e). (B) Influence of pH value on the fluorescence intensities of CDs and EB in CDs–EB–DNA system. CDs: 20 μL; EB: 100 μM; DNA: 50 μM. (C) Influence of pH value on the ratio of the fluorescence intensity of CDs to the fluorescence intensity of EB in CDs–EB–DNA system. CDs: 20 μL; EB: 100 μM; DNA: 50 μM.

Fig. 6. Fluorescence spectra of CDs–EB system in different concentrations of DNA (a ~ m): 0; 1; 4; 7; 10; 20; 30; 40; 50; 60; 70; 80; 100 μM. Insert: linear relationship between I_{EB} / I_{CDs} and DNA concentration in the range of 1.0 μM ~ 100 μM. CDs: 20 μL; EB: 300 μM; pH: 8.0.

Fig. 7. (A) UV-vis absorption spectra of CDs, EB and CDs–EB system; the difference absorption

spectra between CDs–EB system and EB, and the summed absorption spectrum between CDs and EB, respectively. CDs: 20 μL; EB: 30 μM. (B) UV-vis absorption spectra of DNA, EB and EB–DNA system, and the difference absorption spectra between EB–DNA system and DNA, respectively. DNA: 10 μM; EB: 30 μM.

Fig. 8. Fluorescence decay traces of CDs alone (a), CDs–EB system (b), and CDs–EB–DNA system (c). All measurements were made at λ_{em} = 447 nm. τ is the fluorescence decay time of CDs, a is the fractional contribution and b is the normalized preexponential factor, respectively. CDs: 20 μL; EB: 300 μM; DNA: 100 μM.

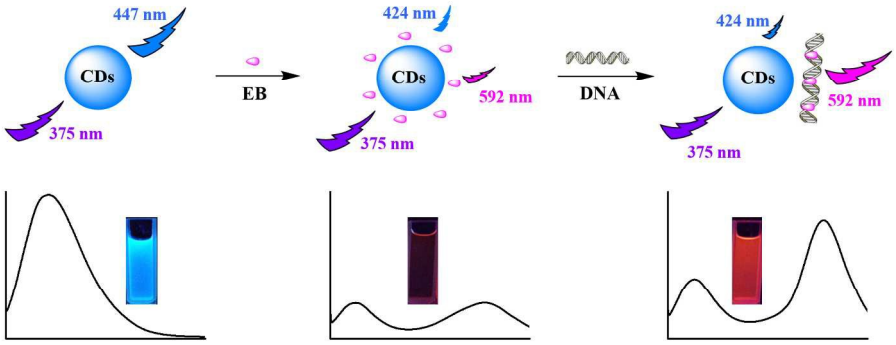

Scheme 1. Principle of DNA determination using CDs-based retiometric fluorescent nanosensor.
374x156mm (150 x 150 DPI)

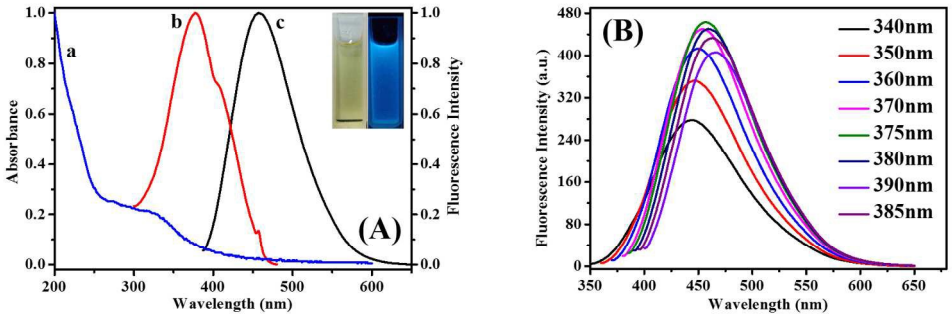

Fig. 1. (A) UV-vis absorption spectra of CDs (a), the excitation spectrum of CDs at λem = 447 nm (b), and the emission spectrum of CDs at λex = 375 nm (c). Insert: Photograph of CDs under the radiation of white light (Left) and 365 nm UV lamp (Right). (B) Fluorescence spectra of CDs at different excitation wavelength.
313x118mm (150 x 150 DPI)

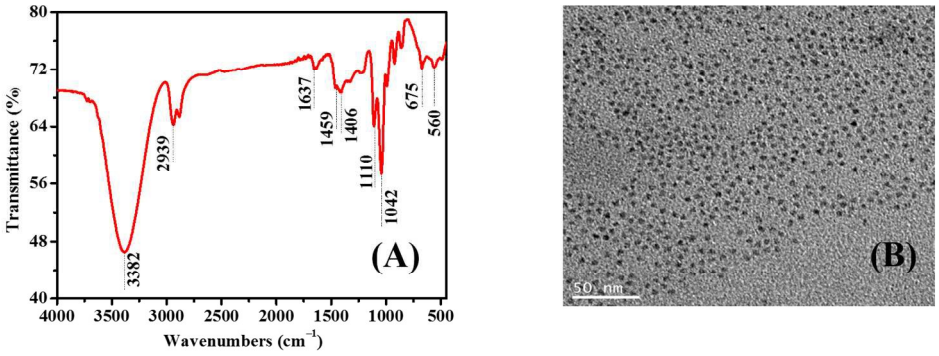

Fig. 2. (A) FT-IR spectrum of CDs. (B) TEM image of CDs.
279x113mm (150 x 150 DPI)

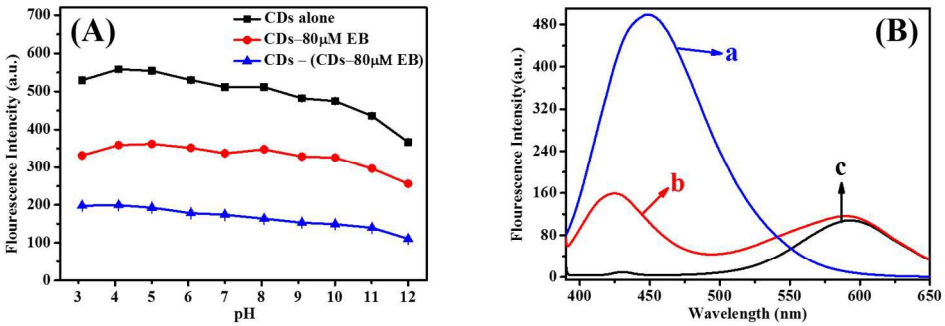

Fig. 3. (A) Influence of pH value on the fluorescence intensity of CDs alone, the fluorescence intensity of CDs–EB system, and the difference between the CDs alone and CDs–EB system. CDs: 20 μL; EB: 80 μM. (B) The control experiment. CDs alone (a); CDs–EB system (b); EB alone (c). CDs: 20 μL; EB: 150 μM.
299x116mm (150 x 150 DPI)

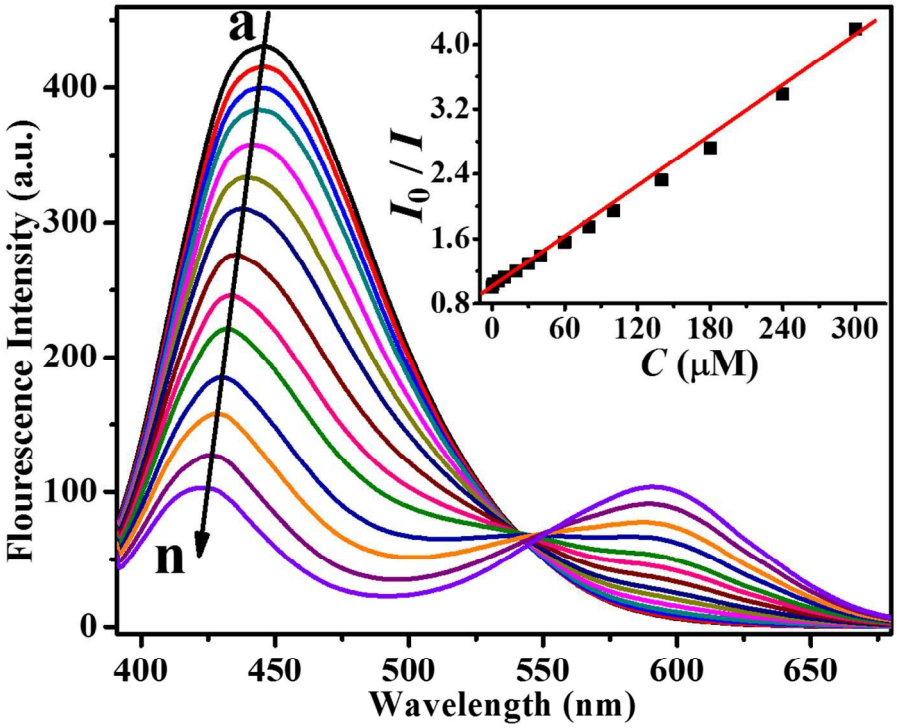

Fig. 4. Fluorescence spectra of CDs in different concentrations of EB (a ~ n): 0; 1; 5; 10; 20; 30; 40; 60; 80; 100; 140; 180; 240; 300 μM. Insert: linear relationship between I0 / I and EB concentration in the range of 1.0 μM ~ 300 μM. CDs: 20 μL; pH: 4.0.
220x176mm (150 x 150 DPI)

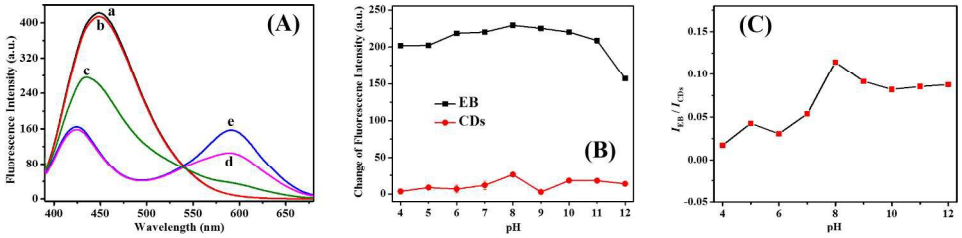

Fig. 5. (A) The fluorescence spectra of CDs alone (a), CDs–DNA (b), CDs–EB (c, d) and CDs–EB–DNA (e). CDs: 20 μL; EB: 100 μM (c) and 300 μM (d, e); DNA: 10 μM (b, e). (B) Influence of pH value on the fluorescence intensities of CDs and EB in CDs–EB–DNA system. CDs: 20 μL; EB: 100 μM; DNA: 50 μM. (C) Influence of pH value on the ratio of the fluorescence intensity of CDs to the fluorescence intensity of EB in CDs–EB–DNA system. CDs: 20 μL; EB: 100 μM; DNA: 50 μM.
412x116mm (150 x 150 DPI)

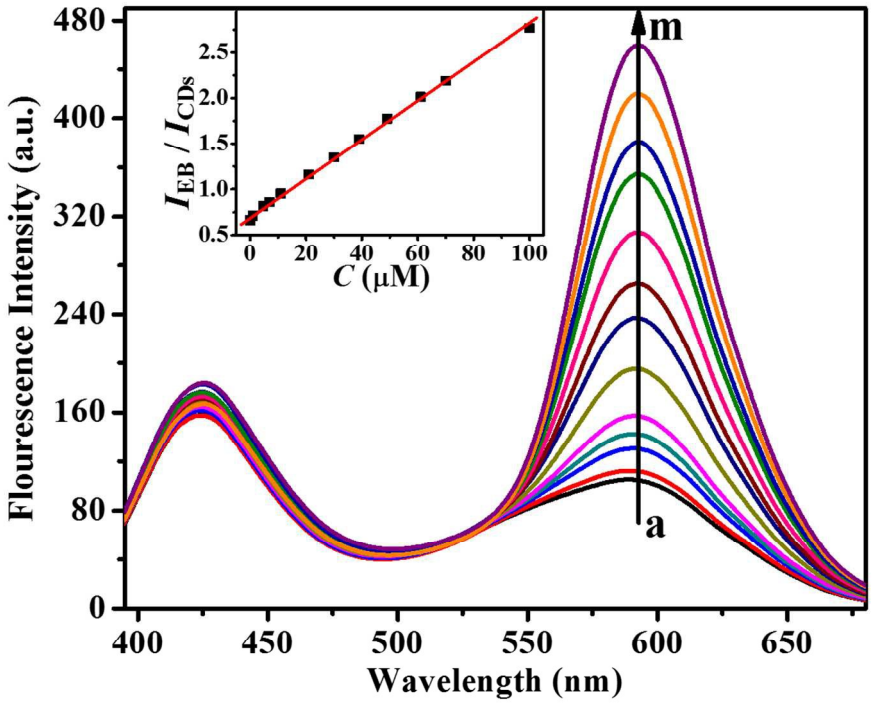

Fig. 6. Fluorescence spectra of CDs–EB system in different concentrations of DNA (a ~ m): 0; 1; 4; 7; 10; 20; 30; 40; 50; 60; 70; 80; 100 μM. Insert: linear relationship between IEB / ICDs and DNA concentration in the range of 1.0 μM ~ 100 μM. CDs: 20 μL; EB: 300 μM; pH: 8.0.
228x180mm (150 x 150 DPI)

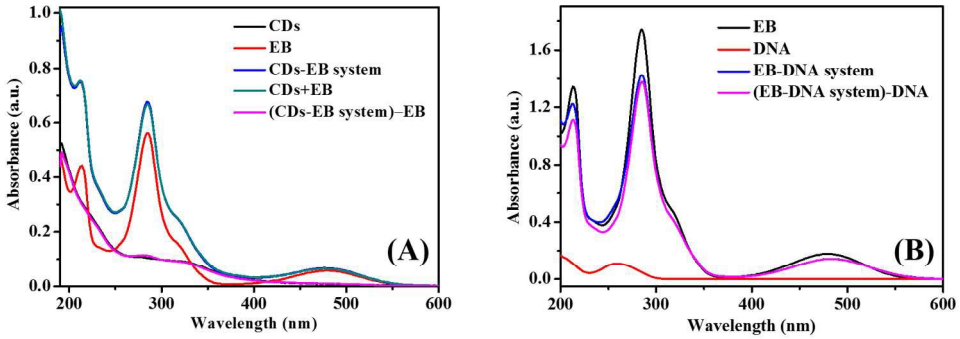

Fig. 7. (A) UV-vis absorption spectra of CDs, EB and CDs–EB system; the difference absorption spectra between CDs–EB system and EB, and the summed absorption spectrum between CDs and EB, respectively. CDs: 20 μL; EB: 30 μM. (B) UV-vis absorption spectra of DNA, EB and EB–DNA system, and the difference absorption spectra between EB–DNA system and DNA, respectively. DNA: 10 μM; EB: 30 μM.
319x121mm (150 x 150 DPI)

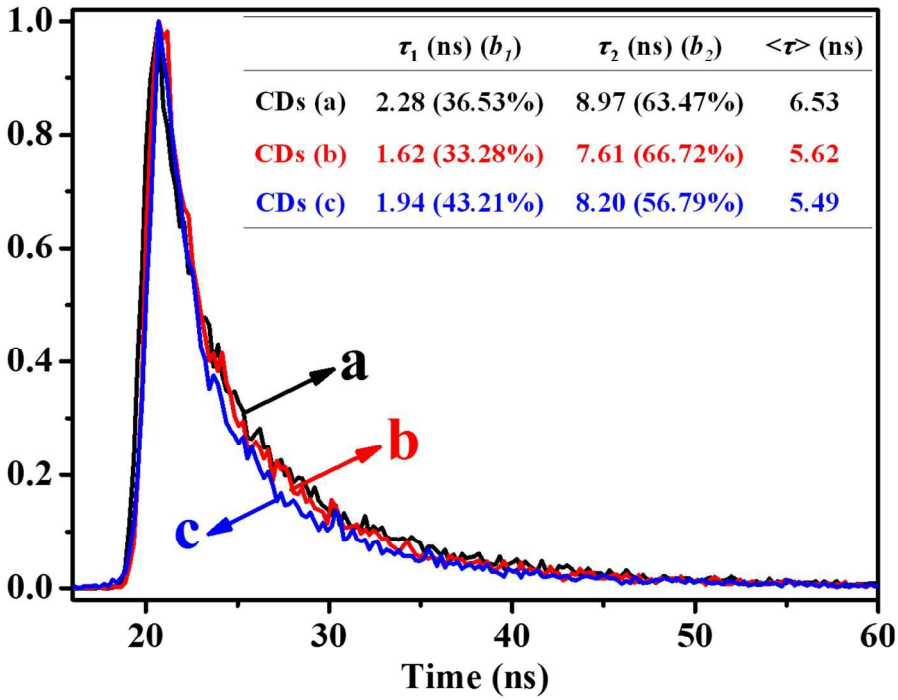

Fig. 8. Fluorescence decay traces of CDs alone (a), CDs–EB system (b), and CDs–EB–DNA system (c). All measurements were made at λem = 447 nm. τ is the fluorescence decay time of CDs, a is the fractional contribution and b is the normalized preexponential factor, respectively. CDs: 20 μL; EB: 300 μM; DNA: 100 μM.
235x180mm (150 x 150 DPI)

Table 1. Effect of coexisting foreign substances for DNA determination [a].

Foreign substances	Concentration coexisting (μM)	Change of FL Intensity (%)	Foreign substances	Concentration coexisting (μM)	Change of FL Intensity (%)
$CaCl_2$	1000	+2.0	L-Tyrosine	500	+3.2
$ZnCl_2$	300	+1.6	L-Glycine	1000	+2.7
$MgCl_2$	1000	+0.8	L-Glutamine	500	+2.0
$FeSO_4$	200	+4.1	L-Cysteine	200	+2.3
GSSG	300	+0.9	L-Methionine	80	+2.6
GSH	300	+0.4	L-Serine	700	+3.5
L-Asparagine	300	+3.7	L-Valine	200	–0.6
L-Throenine	1000	+2.1	L-Histidine	1000	–0.8
L-Arginine	1000	+2.0	L-Glutamic acid	70	+4.1
L-Proline	1000	–0.3	L-Alanine	1000	+1.5
L-Aspartic acid	900	+2.5	L-Lysine	500	+0.1
L-Phenylalanine	1000	+2.0	AA	1000	–0.5
Trypsin	90	+2.3	Lysozyme	100	+0.4
Guannine	900	+4.0	Adenine	1000	+1.4
Cytosine	900	+2.4	Thymine	1000	+3.2
BSA	30	+2.5	HSA	30	+3.1
RNA	40	+5.0			

[a] CDs: 20 μL; EB: 300 μM; DNA: 10 μM.

Table 2. Detection of DNA in synthetic samples (n = 5).

Sample	Added (μM)	Found (μM)	Recovery (%)	R.S.D. (%)
Sample 1 [a]	5	4.95 – 5.01	99.0 – 100.2	1.5
	10	9.84 – 9.98	98.4 – 99.8	2.3
Sample 2 [b]	5	4.88 – 4.95	97.6 – 99.0	1.1
	10	9.83 – 9.94	98.3 – 99.4	1.2
Sample 3 [c]	5	4.93 – 4.96	98.6 – 99.2	1.5
	10	9.96 – 10.03	99.6 – 100.3	0.9
Sample 4 [d]	5	4.95 – 5.03	99.0 – 100.6	0.9
	10	9.92 – 10.18	99.2 – 101.8	1.2
Sample 5 [e]	5	4.97 – 5.05	99.4 – 101.0	1.2
	10	9.97 – 10.06	99.7 – 100.6	1.4
Sample 6 [f]	5	4.86 – 4.93	97.2 – 98.6	0.3
	10	9.93 – 10.01	99.3 – 100.1	1.2
Sample 7 [g]	5	5.03 – 5.07	100.1 – 101.4	0.8
	10	10.02 – 10.21	100.2 – 102.1	2.6

[a] 500 μM $CaCl_2$, 500 μM $MgCl_2$, 100 μM $FeSO_4$, and 100 μM $ZnCl_2$.

[b] 300 μM AA, 300 μM GSSH, 300 μM GSH, 500 μM L-Tyrosine, and 500 μM L-Aspartic acid.

[c] 500 μM L-Asparagine, 500 μM L-Arginine, 500 μM L-Throenine, 500 μM L-Phenylalanine, and 500 μM L-Proline.

[d] 500 μM L-Glycine, 500 μM L-Glutamine, 500 μM L-Cysteine, 500 μM L-Serine, and 80 μM L-Methionine.

[e] 500 μM L-Valine, 500 μM L-Histidine, 500 μM L-Lysine, 500 μM L-Alanine, and 70 μM L-Glutamic acid.

[f] 500 μM Guannine, 500 μM Adenine, 500 μM Cytosine, and 500 μM Thymine.

[g] 50 μM Trypsin, 50 μM Lysozyme, 10 μM BSA, and 10 μM HSA.

Graphical abstract

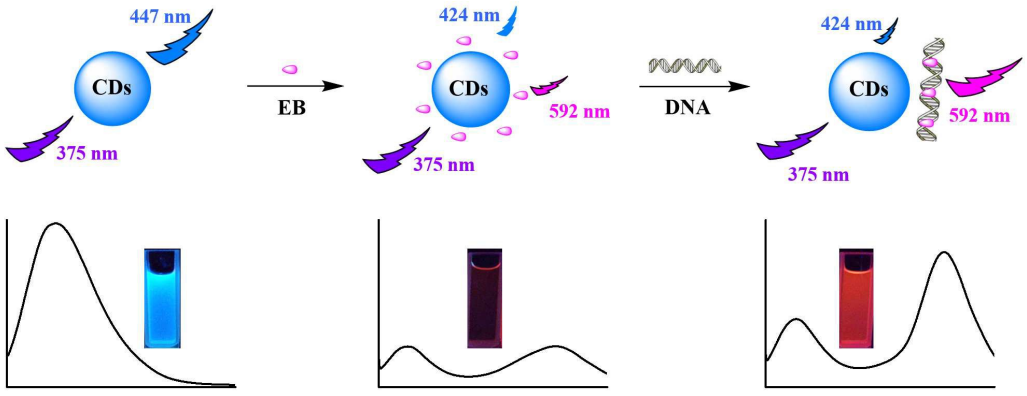

Highlight

A ratiometric nanosensor based on fluorescent carbon dots for label-free and highly selective recognition of DNA.